Lv *et al. Nanoscale Research Letters* (2020) 15:126
https://doi.org/10.1186/s11671-020-03356-3

Nanoscale Research Letters

NANO EXPRESS Open Access

Multilevel Resistive Switching Memory Based on a $CH_3NH_3PbI_{3-x}Cl_x$ Film with Potassium Chloride Additives

Fengzhen Lv*, Kang Ling, Tingting Zhong, Fuchi Liu*, Xiaoguang Liang, Changming Zhu, Jun Liu and Wenjie Kong

Abstract

High-quality $CH_3NH_3PbI_{3-x}Cl_x$ (MAPIC) films were prepared using potassium chloride (KCl) as an additive on indium tin oxide (ITO)-coated glass substrates using a simple one-step and low-temperature solution reaction. The Au/KCl-MAPIC/ITO/glass devices exhibited obvious multilevel resistive switching behavior, moderate endurance, and good retention performance. Electrical conduction analysis indicated that the resistive switching behavior of the KCl-doped MAPIC films was primarily attributed to the trap-controlled space-charge-limited current conduction that was caused by the iodine vacancies in the films. Moreover, the modulations of the barrier in the Au/KCl-MAPIC interface under bias voltages were thought to be responsible for the resistive switching in the carrier injection trapping/detrapping process.

Keywords: Tri-state resistive switching behavior, KCl-doped MAPIC films, Iodine vacancies, Trap-controlled SCLC conduction mechanism

Introduction

As a result of the rapid development in the information storage industry, the high storage density is important for the memory technology. Along with the limit size (∼ 22 nm) of silicon-based memories is approaching, it is difficult to obviously enhance the storage density through further scaling down the device size. Thus, the multilevel storage is an effective alternative approach to enhance the storage density [1, 2]. Among various types of modern memories, resistive switching random access memory (ReRAM) has attracted remarkable attention owing to its simple cell architecture, fast programming speed, high storage density, and low power consumption [3–6]. The ability of multilevel resistive switching (RS) effect has been reported in various inorganic materials [7–10]. Although they possess excellent memory performance, the complex fabrication process and rigidity hinder their development for ReRAM. Most recently, organometal halide perovskites (OHPs) have attracted a great deal of attention in the ReRAM due to their high flexibility, tunable band gaps, and large absorption coefficients [11–15]. Additionally, OHPs have highly defect-tolerant, facile, and cost-effective solution-processed methods that can be adopted to fabricate the OHPs layers [16, 17]. However, OHP-based ReRAM suffers from poor endurance and retention performance. These drawbacks are related to the poor quality of OHP films [18, 19]. In the most recent studies, potassium halides have been proposed as additives to effectively reduce the grain boundaries and compensate for defects in OHPs, to improve optoelectronic properties of OHPs [19–21]. Nevertheless, the RS behavior in potassium halide-doped OHPs has not been extensively reported.

In this study, we prepared $CH_3NH_3PbI_{3-x}Cl_x$(MAPIC) films with the potassium chloride (KCl) additive on indium tin oxide (ITO)-coated glass substrates using a one-step low-temperature solution treatment. Distinct

*Correspondence: lvfzh17@mailbox.gxnu.edu.cn; liufuchi@gxnu.edu.cn
College of Physics and Technology, Guangxi Normal University, Yucai Road, 541000 Guilin, China

Springer Open

© The Author(s). 2020 **Open Access** This article is licensed under a Creative Commons Attribution 4.0 International License, which permits use, sharing, adaptation, distribution and reproduction in any medium or format, as long as you give appropriate credit to the original author(s) and the source, provide a link to the Creative Commons licence, and indicate if changes were made. The images or other third party material in this article are included in the article's Creative Commons licence, unless indicated otherwise in a credit line to the material. If material is not included in the article's Creative Commons licence and your intended use is not permitted by statutory regulation or exceeds the permitted use, you will need to obtain permission directly from the copyright holder. To view a copy of this licence, visit http://creativecommons.org/licenses/by/4.0/.

multilevel RS behavior was achieved by the Au/KCl-MAPIC/ITO/glass devices at different set voltages (V_{SETs}). Subsequently, we analyzed the non-volatile RS effect in the Au/KCl-MAPIC/ITO/glass memory device. The electrical conductive behavior is primarily attributed to the trap-controlled space-charge-limited current (SCLC) conduction mechanism based on the variation of iodine vacancies in the KCl-MAPIC films. Moreover, the modulations of the barrier at the Au/KCl-MAPIC interface under bias voltages are thought to be responsible for the RS behavior.

Methods

Prior to growing the samples, the ITO/glass substrates (10 mm×10 mm, Luoyang Guluo Glass Co., Ltd.) were cleaned sequentially in acetone, isopropyl alcohol, and deionized water and were dried under a nitrogen gas flow. The perovskite precursor solution was prepared by combining lead iodide (PbI_2, 98%, 370 mg, Shanghai Aladdin Bio-Chem Technology Co., Ltd.), methylammonium iodide (MAI, 99.5%, 130 mg, Shanghai Macklin Biochemical Co., Ltd.), and methylammonium chloride (MACl, 98%, 20 mg, Shanghai Aladdin Bio-Chem Technology Co., Ltd.) with anhydrous *N,N*-dimethylformamide (DMF, >99.5%, 1 mL, Xilong Scientific Co., Ltd.). Subsequently, KCl (>99.5%, 7 mg, Tianjin Guangfu Technology Development Co., Ltd.) was added to the mixed solution. The yellowish precursor solution (0.8 M) was stirred more than 6 h in an argon-filled glove box. Then, the precursor solution was spin-coated on ITO/glass substrates at 3000 rpm for 30 s, as shown in Fig. 1a. After 6 s of spin coating, anhydrous chlorobenzene (100 μL, Shanghai Aladdin Bio-Chem Technology Co., Ltd.) was dropped rapidly onto the surface of the intermediate phase film. The film immediately changed from pale yellow to nut-brown [Fig. 1b, c]. Finally, the sample was heated on a hot plate at 100 °C for 10 min, as shown in Fig. 1d.

Characterization

The crystal structure of the MAPIC films was investigated by X-ray diffractometry (XRD; MiniFlex600, Rigaku, JPN). The chemical element analysis of the films was performed using X-ray photoelectron spectroscopy/ultraviolet photoelectron spectroscopy (XPS/UPS; ESCALAB250Xi, Thermo Fisher Scientific, USA) using Al Kα radiation and a He I source with 21.22 eV. The surface morphology of the MAPIC films was examined using scanning electron microscopy (SEM; FEI Quanta 200). The electrical characterization of the KCl-MAPIC films was performed using a Keithley 2400 SourceMeter controlled by the LabVIEW program.

Results and Discussion

Figure 2a shows the XRD pattern of the KCl-doped MAPIC films. The (110), (220), and (330) sharp peaks are in accordance with the tetragonal phase of the crystallized perovsikte film [12, 22]. Figure 2b depicts the XPS wide scan spectrum of the KCl-MAPIC films. C, Pb, I, N, and K are obviously present in the films. However, the peak of Cl 2*p* core-level can not be clearly observed in the full spectrum. This finding is consistent with the results of previous reports, where a number of Cl atoms that involve in the form of gaseous CH_3NH_3Cl or other gaseous Cl-containing mixtures could easily escape in the annealing step, in order to drive the formation and crystallization of perovskite films [22, 23]. Although the XPS wide scan spectrum shows negligible signals of the Cl 2*p* core level, the narrow scan detects weak signals corresponding to the Cl $2p_{3/2}$ and Cl $2p_{1/2}$ peaks, as shown in Additional file 1: Fig. S1 (Supporting Information). It indicates that there are minute amounts of Cl in the final product of perovskite films. Figure 2c presents the top-view SEM image of the KCl-MAPIC films. It is found that the KCl-doped MAPIC films exhibit a high coverage and is dense. Compared with the porous surface of MAPIC films without the KCl additive (Additional file 1: Fig. S2), KCl as a kind of suitable additive is demonstrated that can enhance the quality of OHP films. It consists to previous reports, in which the alkali metal halides could chelate with Pb^{2+} ions and enhance the crystal growth of lead-halide perovskite films [19, 24]. Figure 2d shows that the thickness of the dense KCl-MAPIC layer is ~ 200 nm.

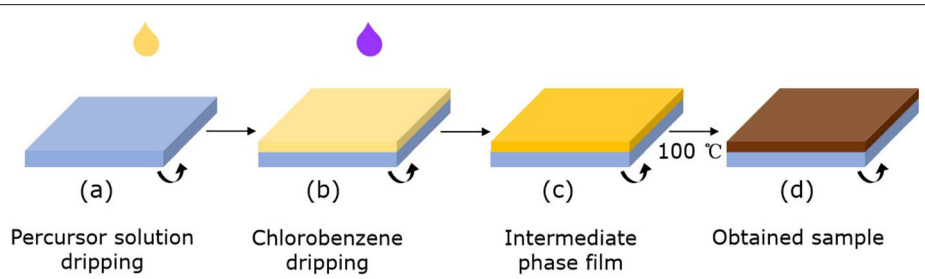

Fig. 1 Solvent engineering procedure for preparing the KCl-doped MAPIC film on the ITO-coated glass substrate

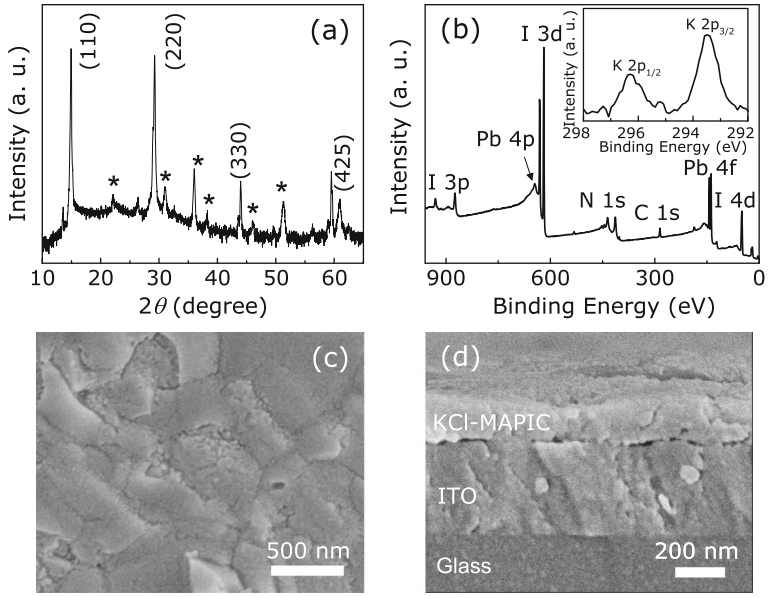

Fig. 2 a XRD spectrum of the as-prepared KCl-doped MAPIC films on the ITO-coated glass substrate. ⋆ represents peaks of the ITO/glass substrate. **b** XPS wide spectrum of the perovskite films. The inset displays the core-level XPS spectrum of K. **c** The top-view and **d** the cross-section SEM images of KCl-MAPIC layers formed on the ITO/glass substrate

Figure 3 shows the current-voltage ($I - V$) characteristics by applying voltage loops to the Au/KCl-MAPIC/ITO/glass devices with periodic sweepings (0 V→0.8 V/1 V→0 V→-0.8 V→0 V). Initially, the device is in a high-resistance state (HRS), and then, the current increases gradually as the positive voltage increases. Subsequently, the memory device transitions from the HRS to different low-resistance states (LRSs) under the two V_{SETs} of 0.8 V and 1 V. The $I - V$ characteristics indicate that the Au/KCl-MAPIC/ITO/glass devices have the multilevel storage potential.

In order to identify the RS performance of Au/KCl-MAPIC/ITO/glass devices, we measured the $I - V$ curves of the devices based on MAPIC films without the KCl additive as references. As shown in Additional file 1: Fig. S3(a), a typical bipolar RS behavior is observed in MAPIC films prepared without the KCl doping, whereas the RS effect is weaker than in KCl-doped MAPIC

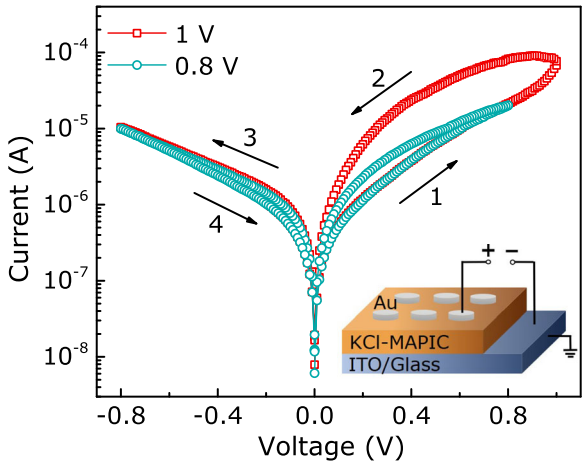

Fig. 3 The semi-logarithmic plots of the $I - V$ curves of Au/KCl-MAPIC/ITO/glass devices in voltage sweeping mode. The inset displays the schematic measurement. Au electrodes with diameters of 300 μm were deposited on the surface of KCl-MAPIC films by magnetron sputtering

films. As exhibited in Additional file 1: Fig. S3(b), the multilevel RS behavior is not been observed in the Au/MAPIC/ITO/glass devices under the V_{SETs} of 0.8 V and 1.0 V. The above results indicate that the KCl additive improves memory properties of the MAPIC-based devices. We surmise that the improvement is related with the enhancement of the films quality. The dense surface of KCl-doped MAPIC films avoided the top electrodes getting deposited in the pores and directly contacting with the bottom electrodes during the preparation process of the devices. So it is helpful to growing the uniform RS structures with the OHP layers [19, 25].

The retention and endurance stability determine the multilevel-storage reliability of the Au/KCl-MAPIC/ITO/glass devices and evaluate the potential application of the devices in the RRAM. Figure 4a displays the endurance cycle dependence of the resistance states in the Au/KCl-MAPIC/ITO/glass devices. Electric pulses of reset voltage (V_{RESET}) and V_{SETs} were alternately applied to the devices (pulse width=0.4 s). After applying the V_{RESET} of −0.8 V, a high resistance state (HRS) was measured at a read voltage (V_r=0.22 V), which was defined as the "OFF state." After applying the V_{SETs} of 0.8 V and 1 V, two different low resistance states (LRSs) were measured at the V_r, which were defined as "level 1" and "level 2," respectively. Above different resistance states can be maintained for up to 140 cycles under electric pulses. Figure 4b displays the retention property of the Au/KCl-MAPIC/ITO/glass devices. After applying the V_{RESET}, the device showed "OFF state" at the V_r and maintained "OFF state" after the V_{RESET} was removed. After applying V_{SETs}, the device exhibited "level 1" and "level 2" at the V_r; these two LRSs remained even though V_{SETs} were removed. Each resistance state is stable for over 1000 s without operation voltages. Therefore, the potential of the multilevel memory has been demonstrated in the Au/KCl-MAPIC/ITO devices.

In order to investigate the mechanism of RS behaviors in the Au/MAPIC/ITO/glass devices, the relationship of log I versus log V was plotted. As shown in Fig. 5a, in the initial positive bias region from 0 to 0.2 V, the $I-V$ relationship has a slope of ~ 1.01, demonstrating that the conductive behavior follows Ohm's law. With the positive bias increasing (0.2 V$\sim$ 0.6 V), the $I-V$ relationship is $I \propto V^2$ and obeys the SCLC mechanism controlled by single shallow traps. When the forward bias reaches the trap-filled limit voltage (V_{TFL}), the current increases sharply with the bias voltage sweeping and the slope is ~ 8.20, and the $I-V$ relationship obeys the exponential distributed trap-controlled SCL conduction. When the bias reaches V_{SET}, the resistive state changes into the LRS. Even though the positive bias decreases, the resistance still maintains the LRS. As illustrated in Fig. 5b, when the bias sweeps reversely, the Au/KCl-MAPIC/ITO/glass device remains in the LRS, whereas the negative bias crosses V_{RESET} and reaches V^*_{TFL}; the current decreases as the voltage decreases and the relationship of $I-V$ recovers $I \propto V^2$.

In OHP-based ReRAM, it is generally accepted that intrinsic point defects in OHP layers can be responsible for the RS behavior [26]. Thereinto, halide vacancies are readily formed in the OHP films during the lowest solution-based film-deposition process [27]. Among these vacancies, iodine vacancy (V_I) possesses a high mobility due to the lowest activation energy of $\sim$ 0.58 eV [26, 28]. Thus, V_I is assumed to play a major role for the RS conductive behavior in the Au/KCl-MAPIC/ITO/glass devices [29]. Additionally, although the appropriate dosage of KCl additives can enhance the MAPIC film quality, potassium ion doping has been verified that could suppress hysteresis of current in OHP solar cells due to the compensation effect for the defect states at the surface or interface of OHP layers [19, 21, 30]. Thus, the origin of obvious multilevel RS characteristics is hardly attributed to potassium ions in our work. We obtained XPS measurements to verify the hypothesis and analyze the condition of the perovskite layer. Figure 6 illustrates the survey XPS spectra of I 3*d* and Pb 4*f*. The

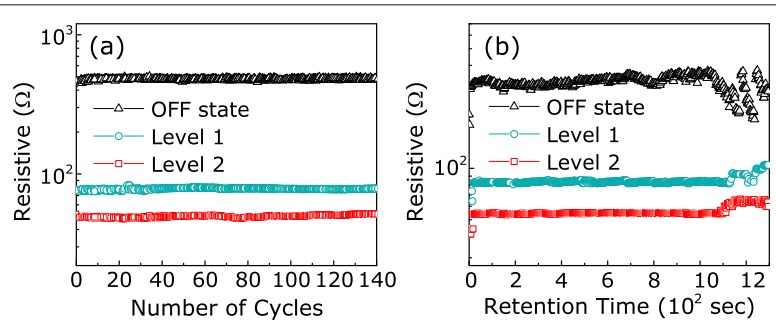

Fig. 4 a Pulse cycles up to 140 times and **b** time up to about 1200 s for HRS and LRS measurements in the Au/KCl-MAPIC/ITO/glass device at room temperature

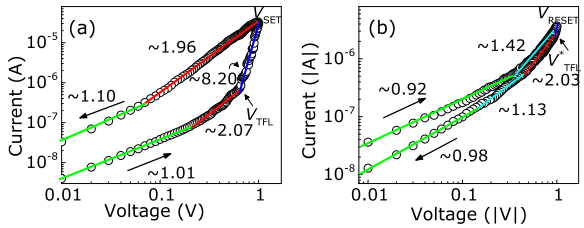

Fig. 5 The fitted lines of log *I*-log *V* plots in the **a** positive and **b** negative voltage regions. The arrows indicate the sweeping direction

peaks located at 631.90 eV and 620.45 eV are consistent with I $3d_{3/2}$ and I $3d_{5/2}$, respectively. The peak positions shift slightly to higher binding energy, which indicates the generation of V_I by heat-driven deiodination [31, 32]. The XPS result in Fig. 6b shows the Pb 4*f* core level spectrum. Two main peaks of Pb $4f_{5/2}$ and Pb $4f_{7/2}$ are observed at 143.18 eV and 138.21 eV, respectively. It is noteworthy that additional small peaks with lower binding energies (141.41 eV and 136.60 eV) with the signature of Pb^0 were detected by XPS [33, 34]. These results indicate that V_I exists in the KCl-doped MAPIC layer.

As shown in Fig. 7a, in a low positive bias region (0< V <0.2 V), the concentration of thermally generated free carriers is higher than injected carriers in the KCl-MAPIC layer, so the $I-V$ relationship obeys Ohm's law:

$$j = qn\mu\frac{V}{d} \tag{1}$$

where j is the transport current density, q is the electric charge, n is the density of the free electrons in thermal equilibrium, μ is the carrier mobility, V is the applied voltage, and d is the media layer thickness. As the forward voltage increases (0.2 V< V < V_{TFL}), the electrons injected from the bottom ITO electrode are captured by V_I in the KCl-MAPIC layer [Fig. 7b]. The $I-V$ relationship follows the functional form:

$$j = \frac{9}{8}\theta\varepsilon_0\varepsilon_r\mu\frac{V^2}{d^3} \tag{2}$$

where θ is the fraction of free carriers, ε_0 is the permittivity of the free space, and ε_r is the dielectric constant of the insulator. This conductive behavior obeys the SCL conduction mechanism, which is controlled by single shallow traps located closely at the conduction band [9]. When the forward voltage increases to V_{TFL}, the electrons trapped are activated and released from traps, whereas additional injected electrons immediately fill in these traps. Thus, the traps are always filled up; the conductive behavior switches to the trap-free SCL conduction. The current exponentially increases with the positive bias increasing. The aforementioned process is known as the trapping process. When the forward voltage reaches V_{SET}, the Au/KCl-MAPIC/ITO cell finally reaches the LRS [Fig. 7c]. The charge traps are filled over time, and the electrons can then hop from trap-to-trap. As the positive bias voltage decreases, the device remains in the LRS due to the high electron concentration in the KCl-MAPIC layer. As illustrated in Fig. 7d, the device still stays in the LRS even though the bias voltage sweeps reversely. Because the trapped electrons cannot be released from the V_I immediately; the carrier concentration remains at a high level. As the negative voltage reaches and crosses V_{RESET}, the device switches from the LRS to the HRS. The trapped electrons are drawn out from the traps; the electron concentration decreases [Fig. 7e]. When the reverse bias decreases to V^*_{TFL}, the current behavior recovers the SCL conduction controlled by single shallow traps. The aforementioned process is known as the detrapping process. As the negative voltage further decreases, the electrons cannot be captured by the traps; the concentration of injected electron concentration is lower than the equilibrium concentration. Therefore, the KCl-MAPIC layer

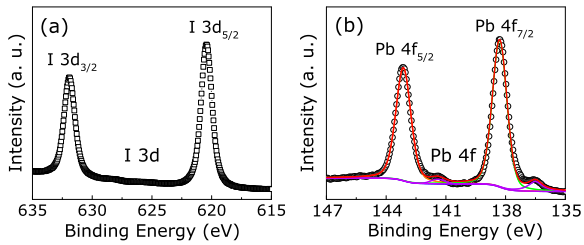

Fig. 6 XPS spectra of **a** I 3*d* and **b** Pb 4*f* core levels of the KCl-doped MAPIC films

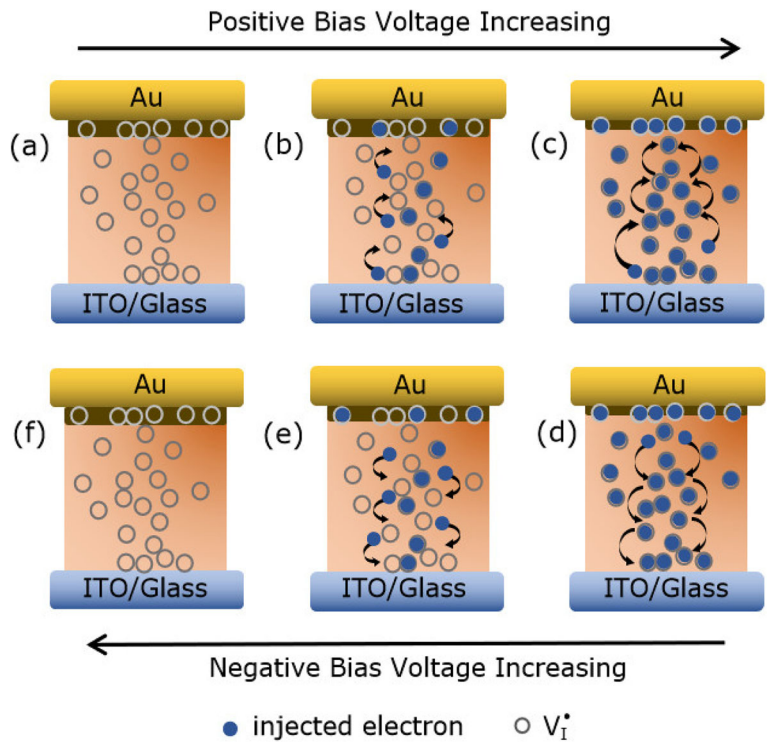

Fig. 7 a–f The schematic of the RS mechanism model in the Au/KCl-MAPIC/ITO/glass cell

returns to the unoccupied trap state; current behavior transits from SCL conduction to Ohmic conduction [Fig. 7f].

Furthermore, according to reports on the transition process of the current under a bias sweep, we surmise that the bias-induced modification of the barrier height and/or width in the Au/KCl-MAPIC/ITO sandwiches also contributed to the resistive switching [22, 35, 36]. UPS was conducted to confirm the conjecture and examine the contact types of the electrodes/perovskite layer. Figure 8a, b shows the cut-off regions of the KCl-MAPIC film and ITO-coated glass, respectively. The work functions of the film and substrate are calculated as 4.42 eV and 4.50 eV, respectively. These values are similar to results obtained in previous reports [22, 36, 37]. Thus, we confirm that a contact between KCl-MAPIC layer and ITO-coated glass is Ohmic due to their similar work functions. However, it is well known that the work function of Au is about 5.0 eV [22, 35]. This value is larger than that of the KCl-MAPIC film. Therefore, a barrier forms at Au/KCl-MAPIC interface. As shown in Fig. 7b, electrons start to drift towards the Au electrode and be captured by the V_i depletion layer near the Au/KCl-MAPIC interface under a positive voltage. When the forward voltage reaches V_{SET}, the holes are full-filled, lead to the Schottky-like barrier lowing, and the depletion layer thinning [Fig. 7c]. The contact between KCl-doped MAPIC layer and Au electrode becomes a quasi-ohmic contact, and the device switches from the HRS to the LRS. As shown in Fig. 7d–f, when the bias sweeps in reverse direction and increases to V_{RESET}, the trapped electrons are pulled out from hole traps and the barrier recovers to the original stat; the electrons

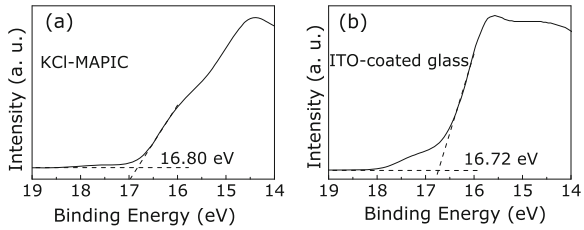

Fig. 8 Cut-off regions of **a** the KCl-MAPIC film and **b** the ITO-coated glass

injected from the Au electrode are obstructed. Thus, the carrier concentration decreases in the KCl-MAPIC layer; the Au/KClMAPIC/ITO device switches from the LRS to the HRS.

Conclusions

High-quality KCl-doped MAPIC films were prepared using the low-temperature one-step solution synthesis. The appropriate dosage of potassium chloride doping could help MAPIC films grow to the good quality with high coverage and dense surface. The memory cells consisting of Au/KCl-MAPIC/ITO/glass exhibited a tri-state RS behavior after applying different V_{SETs} at room temperature. Cycling endurance (>140 cycles) and data retention (≥1000 s) demonstrated that the Au/KCl-MAPIC/ITO/glass devices have the potential for multilevel storage in ReRAM. The analysis of conductive processes revealed the V_i traps-controlled SCLC mechanism contributed to the RS behavior. Furthermore, the modulation of the Au/KCl-MAPIC barrier under the applied bias was also responsible for the resistive state switching in the carrier injection-trapping/detrapping process.

Supplementary information

Supplementary information accompanies this paper at https://doi.org/10.1186/s11671-020-03356-3.

Additional file 1: Supporting Information.

Abbreviations

ReRAM: Resistive switching random access memory; OHPs: Organometal halide perovskites; MAPIC: $CH_3NH_3PbI_{3-x}Cl_x$; KCl: Potassium chloride; ITO: Indium tin oxide; RS: Resistive switching; $I-V$: Current-voltage; LRS: Low resistance states; HRS: High resistance state; V_{SET}: Set voltage; V_{RESET}: Reset voltage; V_r: Read voltage; V_I: Iodine vacancy; SCLC: Space-charge-limited current; V_{TFL}: Trap-filled limit voltage; XRD: X-ray diffractometry; XPS: X-ray photoelectron spectroscopy; UPS: Ultraviolet photoelectron spectroscopy; SEM: Scanning electron microscopy

Acknowledgements

The authors thank the financial support provided by the National Natural Science Foundation of China, Natural Science Foundation of Guangxi Province, and Scientific Research and Technology Development Program of Guilin.

Authors' Contributions

Fengzhen Lv provided the conceptualization, guided the experiments, conducted the data analysis, and prepared the original draft. Kang Ling conducted the experimental process and participated in the data discussion. Tingting Zhong participated in the experimental process. Fuchi Liu, Xiaoguang Liang, Changming Zhu, Jun Liu, and Wenjie Kong provided guidance for the experiments and participated in the revision of the manuscript. The authors read and approved the final manuscript.

Funding

This work was financially supported by the National Natural Science Foundation of China (No.11664003), Natural Science Foundation of Guangxi Province (No. 2018GXNSFAA294021, 2018GXNSFBA281073, 2018GXNSFBA138007), and the Scientific Research and Technology Development Program of Guilin (No.2016012002).

Availability of Data and Materials

All data generated and analyzed during this study are included in this article and the attached supporting information.

Competing Interests

The authors declare that they have no competing interests.

Received: 26 February 2020 Revised: 15 May 2020 Accepted: 18 May 2020
Published online: 05 June 2020

References

1. Wang Y, Liu Q, Long SB, Wang W, Wang Q, Zhang MH, Zhang S, Li YT, Y ZQ, Yang JH, Liu M (2010) Investigation of resistive switching in Cu-doped HfO_2 thin film for multilevel non-volatile memory applications. Nanotechnology 21:045202
2. Lee JS, Kim YM, Kwon JH, Sim JS, Shin HJ, Sohn BH, Jia QX (2011) Multilevel data storage memory devices based on the controlled capacitive coupling of trapped electrons. Adv Mater 26:2064–2068
3. Waser R, Aono M (2007) Nanoionics-based resistive switching memories. Nat Mater 6:833–843
4. Ismail M, Talib I, Rana AM, Akbar T, Jabeen S, Lee JJ, Kim SJ (2018) Effect of bilayer CeO_{2-x}/ZnO and ZnO/CeO_{2-x} heterostructures and electroforming polarity on switching properties of non-volatile memory. Nanoscale Res Lett 13(318):1–10
5. Zahoor F, Zulkifli TZA, Khanday FA (2020) Resistive random access memory (RRAM): an overview of materials, switching mechanism, performance, multilevel cell (MLC) storage, modeling, and applications. Nanoscale Res Lett 15(90):1–26
6. Ding XX, Feng YL, Huang P, Liu LF, Kang JF (2019) Low-power resistive switching characteristic in HfO_2/TiO_x bi-Layer resistive random-access memory. Nanoscale Res Lett 14(157):1–7
7. Zhou WP, Xiong YQ, Zhang ZM, Wang DH, Tan WS, Cao QQ, Qian ZH, Du YW (2016) Multilevel resistance switching memory in $La_{2/3}Ba_{1/3}MnO_3$/0.7Pb($Mg_{1/3}Nb_{2/3}$)O_3-0.3$PbTiO_3$(011) heterostructure by combined straintronics-pintronics. ACS Appl Mater Interfaces 8:5424–5431
8. Huang RM, Yan XZ, Ye S, Kashtiban R, Beanland R, Morgan KA, Charlton MDB, Groot CHK (2017) Compliance-free $ZrO_2/ZrO_{2-x}/ZrO_2$ resistive memory with controllable interfacial multistate switching behaviour. Nanoscale Res Lett 12(384):1–9
9. Lv FZ, Ling K, Wang WF, Chen P, Liu FC, Kong WJ, Zhu CM, Liu J, Long LZ (2019) Multilevel resistance switching behavior in $PbTiO_3$/Nb:$SrTiO_3$(100) heterostructure films grown by hydrothermal epitaxy. J Alloy Compound 778:768–773
10. Wu L, Liu HX, Li JB, Wang SL, Wang X (2019) A multi-level memristor based on Al-doped HfO_2 thin film. Nanoscale Res Lett 14(177):1–7
11. Hwang SK, Lee JM, Kim SJ, Park JS, Park H, Ahn CW, Lee KJ, Lee T, Kim SO (2012) Flexible multilevel resistive memory with controlled charge trap B- and N-doped carbon nanotubes. Nano Lett 12:2217–2221
12. Yoo EJ, Lyu MQ, Yun J-H, Kang CJ, Choi YJ, Wang LZ (2015) Resistive switching behavior in organic–inorganic hybrid $CH_3NH_3PbI_{3-x}Cl_x$ perovskite for resistive random access memory devices. Adv Mater 27:6170–6175
13. Lv FZ, Gao CX, Zhou H-A, Zhang P, Mi K, Liu XX (2016) Nonvolatile bipolar resistive switching behavior in the perovskite-like $(CH_3NH)_3FeCl_4$. ACS Appl Mater Interfaces 8:18985–18990
14. Hwang B, Lee JS (2018) Lead-free, air-stable hybrid organic–inorganic perovskite resistive switching memory with ultrafast switching and multilevel data storage. Nanoscale 10:8578–8584
15. Zhao XN, Xu HY, Wang ZQ, Lin Y, Liu YC (2019) Memristors with organic-inorganic halide perovskites. Info Mat 1:183–210
16. Shan YY, Lyu ZS, Guan XW, Younis A, Yuan GL, Wang JL, Li S, Wu T (2018) Solution-processed resistive switching memories based on hybrid organic-inorganic materials and composites. Phys Chem Chem Phys 20:23837–23846
17. Cheng XF, Qian WH, Wang J, Yu C, He JH, Li H, Xu QF, Chen DY, Li NJ, Lu JM (2019) Environmentally robust memristor enabled by lead-free double perovskite for high-performance information storage. Small 49:1–8
18. Choi J, Han JS, Hong K, Kim SY, Jang HW (2018) Organic-inorganic hybrid halide perovskites for memories, transistors, and artificial synapses. Adv Mater 42:1–21

19. Shih CF, Wu HT, Tsai WL, Leu CC (2019) Improvement of resistive memory properties of poly(3,4-ethylenedioxythiophene):poly(styrenesulfonate)/$CH_3NH_3PbI_3$ based device by potassium iodide additives. J Alloy Compound 783:478–485
20. Zhao WG, Yao Z, Yu FY, Yang D, Liu SZ (2018) Alkali metal doping for improved $CH_3NH_3PbI_3$ perovskite solar cells. Adv Sci 5:1–7
21. Abdi-Jalebi M, Andaji-Garmaroudi Z, Cacovich S, Stavrakas C, Philippe B, Richter JM, Alsari M, Booker EP, Hutter EM, Pearson AJ, Lilliu S, Savenije TJ, Rensmo H, Divitini G, Ducati C, Friend RH, Stranks SD (2018) Maximizing and stabilizing luminescence from halide perovskites with potassium passivation. Nature 555:497–501
22. Zhou FC, Liu YH, Shen XP, Wang MY, Yuan F, Chai Y (2018) Low-voltage, optoelectronic "$CH_3NH_3PbI_{3-x}Cl_x$" memory with integrated sensing and logic operations. Adv Funct Mater 1800080:1–8
23. Yu H, Wang F, Xie FY, Li WW, Chen J, Zhao N (2014) The role of chlorine in the formation process of "$CH_3NH_3PbI_{3-x}Cl_x$" perovskite. Adv Funct Mater 24:7102–7108
24. Boopathi KM, Mohan R, Huang TY, Budiawan W, Lin MY, Lee CH, Hod KC, Chu CW (2016) Synergistic improvements in stability and performance of lead iodide perovskite solar cells incorporating salt additives. J Mater Chem A 4:1591–1597
25. Song HJ, Wang ZJ, Wang JB, Zhong XL (2018) Unipolar resistive switching in porous perovskite-like $Bi_{3.15}Nd_{0.85}Ti_3O_{12}$ thin films. J Mater Sci-Mater El 8:6660–6665
26. Kim HJ, Han JS, Kim SG, Kim SY, J HW (2019) Halide perovskites for resistive random-access memories. J. Mater. Chem. C 18:5226–5234
27. Li C, Guerrero A, Zhong Y, Huettner S (2017) Origins and mechanisms of hysteresis in organometal halide perovskites. J Phys-Condens Mat 29:1–20
28. Yamada N, Ino R, Ninomiya Y (2016) Truly transparent p-Type γ-CuI thin films with high hole mobility. Chem Mater 28:4971–4981
29. Zhu X, Lee J, Lu WD (2017) Iodine vacancy redistribution in organic–inorganic halide perovskite films and resistive switching effects. Adv Mater 29:1–8
30. Zheng F, Chen WJ, Bu TL, Ghiggino KP, Huang FZ, Cheng YB, Tapping P, Kee TW, Jia BH, Wen XM (2019) Triggering the passivation effect of potassium doping in mixed-cation mixed-halide perovskite by light illumination. Adv Energy Mater 9:1–11
31. Liu A, Zhu HH, Park WT, Kang SJ, Xu Y, Kim MG, Noh YY (2018) Room-temperature solution-synthesized p-Type Copper(I) iodide semiconductors for transparent thin-film transistors and complementary electronics. Adv Mater 34:1–7
32. Zi M, Li J, Zhang ZC, Wang XS, Han J, Yang XP, Qiu ZW, Gong HB, Ji ZW, Cao BQ (2015) Effect of deposition temperature on transparent conductive properties of γ-CuI film prepared by vacuum thermal evaporation. Phys Status Solidi A 212:1466–1470
33. Liu T, Su PY, Liu L, Wang J, Feng S, Zhang JJ, Xu R, Yang HB, Fu WY (2019) An ionic compensation strategy for high performance mesoporous perovskite solar cells: healing defects with tri-iodide ions in a solvent vapor annealing process. J Mater Chem A 7:353–362
34. Das C, Wussler M, Hellmann T, Mayer T, Jaegermann W (2018) In situ XPS study of the surface chemistry of MAPI solar cells under operating conditions in vacuum. Phys Chem Chem Phys 20:17180–17187
35. Guan XW, Hu WL, Haque MA, Wei NN, Liu ZX, Chen AT, Wu T (2018) Light-responsive ion-redistribution-induced resistive switching in hybrid perovskite schottky junctions. Adv Funct Mater 28:1704665
36. How GTS, Talik NA, Kar YB, Nakajima H, Tunmee S, Tong GB (2018) Multiple resistive switching behaviours of $CH_3NH_3PbI_3$ perovskite film with different metal electrodes. Appl Surf Sci 473:194–202
37. Yoo EJ, Lyu MQ, Yun JH, Kang CJ, Choi YJ, Wang LZ (2016) Bifunctional resistive switching behavior in an organolead halide perovskite based Ag/$CH_3NH_3PbI_{3-x}Cl_x$/FTO structure. J Mater Chem C 4:7824

Publisher's Note

Springer Nature remains neutral with regard to jurisdictional claims in published maps and institutional affiliations.

Submit your manuscript to a SpringerOpen journal and benefit from:

- ► Convenient online submission
- ► Rigorous peer review
- ► Open access: articles freely available online
- ► High visibility within the field
- ► Retaining the copyright to your article

Submit your next manuscript at ► springeropen.com